Hindawi Publishing Corporation
Advances in Condensed Matter Physics
Volume 2013, Article ID 104806, 13 pages
http://dx.doi.org/10.1155/2013/104806

Review Article

Understanding Multiferroic Hexagonal Manganites by Static and Ultrafast Optical Spectroscopy

Yu Ting Wang,[1] Chih Wei Luo,[1] and Takayoshi Kobayashi[1,2]

[1] *Department of Electrophysics, National Chiao Tung University, Hsinchu 30010, Taiwan*
[2] *Advanced Ultrafast Laser Research Center, University of Electro-Communications, Chofugaoka 1-5-1, Chofu, Tokyo 182-8585, Japan*

Correspondence should be addressed to Chih Wei Luo; cwluo@mail.nctu.edu.tw

Received 25 June 2012; Revised 19 January 2013; Accepted 28 January 2013

Academic Editor: R. N. P. Choudhary

Multiferroic hexagonal manganites $ReMnO_3$ studied by optics are reviewed. Their electronic structures were revealed by static linear and nonlinear spectra. Two transitions located at ~1.7 eV and ~2.3 eV have been observed and attributed to the interband transitions from the lower-lying $Mn^{3+}d_{xy}/d_{x^2-y^2}$ and d_{xz}/d_{yz} states to the $Mn^{3+}d_{3z^2-r^2}$ state, respectively. These so-called d-d transitions exhibit a blueshift as decreasing temperatures and an extra blueshift near T_N. This dramatic change indicates that the magnetic ordering seriously influences the electronic structure. On the other hand, the ultrafast optical pump-probe spectroscopy has provided the important information on spin-charge coupling and spin-lattice coupling. Because of the strongly correlation between electronic structure and magnetic ordering, the amplitude of the initial rising component in $\Delta R/R$ shows striking changes at the vicinity of T_N. Moreover, the coherent optical and acoustic phonons were observed on optical pump-probe spectroscopy. Both the amplitude and dephasing time of coherent phonons also exhibit significant changes at T_N, which provide the evidence for spin-lattice interaction in these intriguing materials.

1. Introduction

Multiferroic materials [1–4] with the coexistence of various ferroic order (ferromagnetic, ferroelectric, or ferroelastic) have attracted great attention in condensed matter research due to their great potential for applications in the fields of oxide electronics, spintronics, and even the green energy devices for reducing the power consumption. With multiferroic oxides (in single phase), the coupling interaction among various order parameters causes the so-called magnetoelectric effect [5–10]. In this, a polarization can be induced by applying a magnetic field or a magnetization can be induced by applying an electric field. Although the properties of electricity and magnetism were combined into one common discipline by the Maxwell equations, the electric and magnetic orderings in solid-state materials are always considered separately. This is because that the electric charges of electrons and ions are responsible for the charge effects, whereas the electron spins govern the magnetic properties.

Prellier et al. [11] classified the characteristics of multiferroic materials into three categories. The first is Bi-based compounds, such as $BiMnO_3$ and $BiFeO_3$. The second is perovskites and related $ReMnO_3$ compounds (Re = Y, Ho, Er, Tm, Yb, and Lu). The third is $ReMn_2O_5$ (Re is rare earth element). Additionally, Cheong and Mostovoy [12] summarized the classification of ferroelectrics into "proper" and "improper" according to their mechanisms of inversion symmetry breaking. In proper ferroelectrics, the main driving force toward the polar state was associated with the electronic pairing. On the other hand, the induced polarization in improper ferroelectrics involves a more complex lattice distortion or other accidental orderings. For example, the hexagonal manganite $ReMnO_3$ compounds show a lattice distortion to enlarge their unit cell, which is the so-called geometric ferroelectricity [13–15].

The aim of this paper is to understand the multiferroic hexagonal manganites studied by some optical techniques. In Section 2, the overall features of manganites are introduced.

The structure of rare earth manganite is strongly depending on the size of rare earth and also temperature. The environment of Mn ions significantly affects its electronic structure which was investigated by static linear and nonlinear spectra in Section 3. Section 4 is the main part of this paper. The ultrafast spectroscopies demonstrate the interaction between electron, phonon, and spin systems on multiferroic hexagonal manganites. Finally, the summary and future outlook will be given in Section 5.

2. The Characteristics of Multiferroic Manganites $ReMnO_3$

Recently, multiferroic rare earth manganites ($ReMnO_3$) have attracted a great deal of attention due to their manifestations of intriguing and significant couplings between the magnetic and electric order parameters. Generally, $ReMnO_3$ has two kinds of multiferroic structures, that is, hexagonal and orthorhombic. The rare earth (Re^{3+}) ionic size shrinks from 1.11 Å to 0.94 Å with decreasing the atomic number and reducing the electrons residing in the 4f orbit, called the lanthanum contraction effect. The rare earth ions (Re^{3+}) have closely chemical properties because the same electronic configurations of $5s^2 5p^6$ for outermost electrons. The coexistence of ferroic orders in $ReMnO_3$ with hexagonal (smaller ionic radius of rare earth Re = Sc, Y, and from Ho to Lu) or orthorhombic (larger ionic radius of rare earth Re = La to Dy) (shown in Figure 1) structure yields complex physics in the intimate interactions among charge, orbital, lattice, and spin degrees of freedom. It also has fascinating physical properties which might lead to promising applications. The orthorhombic structure with a *Pnma* space group forms the stable crystal structure of $ReMnO_3$ perovskite oxides with Re = La to Dy, which belongs to the magnetic ferroelectrics induced by magnetic ordering [8, 16]. Furthermore, another family of compounds with smaller ionic size (for Re = Y, Ho, Er, Yb, Lu, etc.) forms the stable hexagonal structure with $P6_3cm$ space group. The critical point of the structure transition is located near $YMnO_3$ (Y^{3+} = 1.06 Å) and $HoMnO_3$ (Ho^{3+} = 1.05 Å). Consequently, the crystal structures of these two families have been transformed from hexagonal to orthorhombic (or vice versa) by many experimental techniques, for example, high-temperature and high-pressure processes [17, 18], chemical solution deposition (CSD) [19], the metal-organic chemical vapor deposition (MOCVD) [20], molecular beam epitaxy (MBE) [21], sputtering [22], and pulsed laser deposition (PLD) [16, 23].

In the following, we are going to focus on recent studies on the multiferroic hexagonal manganites ($ReMnO_3$, Re = rare earth) which have properties similar to various rare-earth elements, both electric transportation or magnetic behaviors. For example, the hexagonal $HoMnO_3$ has ferroelectric ordering at Curie temperature T_C = 875 K, the antiferroicmagnetic (AFM) Mn^{3+} ordering at Néel temperature T_N = 76 K, and the magnetic Ho^{3+} ordering at T_{Ho} = 4.6 K, in which the magnetically active ions are the high spin Mn^{3+} ($3d^4$, $S = 2$) and Ho^{3+} ($4f^{10}$) [5, 14, 33, 40–45]. The ferroelectricity in magnetoelectric $ReMnO_3$ is caused by

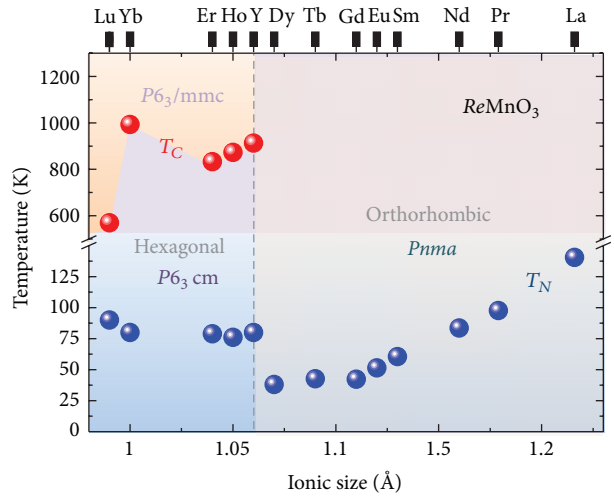

FIGURE 1: Lattice structure in $ReMnO_3$ as a function of the size of the rare-earth elements [11, 24–29].

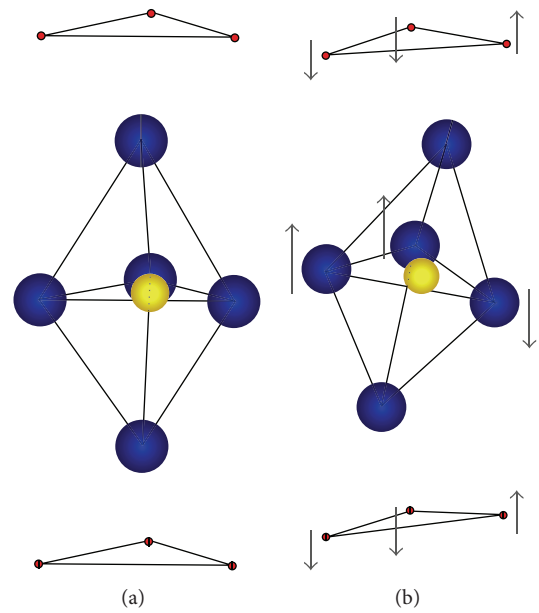

FIGURE 2: Schematic of MnO_5 bipyramid above and below T_C, respectively. (a) Centrosymmetric structure with space group $P6_3$/mmc and (b) noncentrosymmetric with $P6_3cm$ space group. The arrows indicate atomic displacements with respect to the centrosymmetric structure [14, 30]. (Red: Re, blue: O, yellow: Mn).

a buckling of the layered MnO_5 polyhedral and is accompanied by displacements of the Re ions, which lead to a net electric polarization. In 2004, through X-ray diffraction and first principle density functional calculations, Van Aken et al. [14] demonstrated the previous scenario in the hexagonal manganite $YMnO_3$, as shown in Figure 2 which presents the "geometric" generation of polarization and describes the tilting of a rigid MnO_5 block with a magnetic Mn atom at the center. The magnetic structure has been studied by various experimental methods, such as neutron diffraction [45, 46] or second harmonic generation (SHG) [33, 47]. In

$P6_3cm$ hexagonal manganites, each Mn^{3+} ion is surrounded by five O^{2-} ions, forming triangular planar sublattices in the basal plane (a-b plane). The magnetic order of Mn^{3+} is mainly dominated by AFM in-plane Mn-O-Mn superexchange interaction. Therefore, the triangular lattice of the Mn atoms exhibits strong geometrical frustration effect [48]. Furthermore, when the temperature cools to near T_N, the strong superexchange leads to a 120° arrangement between neighboring Mn^{3+} spins in the basal plane which breaks the triangular frustration. In addition, the spins of Mn rotate with an angle of 90° at T_{SR} (e.g., for h-$HoMnO_3$, $T_{SR} \sim 33$ K) due to the onset of the AFM order of the Re moments, indicating the interaction between Re^{3+} and Mn^{3+} spins. Another magnetic transition at T_{Re} involves the complete magnetic order of the Re^{3+} ions (e.g., for h-$HoMnO_3$, $T_{Ho} \sim 5$ K).

In addition, there are many studies showing the anomaly around T_N, such as the dielectric constant [49], specific heat measurements [50], and the lattice constant measurements [51], which are attributed to the indirect coupling via lattice strain (spin-lattice coupling). Recently, Lee et al. [52] observed the giant magnetoelastic effect in hexagonal $YMnO_3$ and $LuMnO_3$ by using the high-resolution neutron and synchrotron powder diffraction experiments. They further claimed that the magnetoelectric (ME) coupling can be interpreted by the giant magnetoelastic effect very well in $ReMnO_3$, that is, the magnetic long-range ordering induced the very large displacements of all atoms at T_N. In other words, the magnetoelastic coupling allowed the atoms to undergo an isostructural transition, which has been regarded as the primary source of the magnetoelectric phenomena. In hexagonal $ReMnO_3$, this magnetoelastic effect is two orders of magnitude larger than those appearing in other magnetic materials. Therefore, the gigantic magnetoelastic coupling plays a crucial role in dominating many physical properties in hexagonal $ReMnO_3$.

Femtosecond pump-probe spectroscopy has been established as a protocol for studying the interactions between electrons, phonons, and magnons [35, 53–59] and is therefore employed with these multiferroic $ReMnO_3$ materials to gain insight into the magnetoelastic effect. By measuring the transient reflectivity ($\Delta R/R$) or transmittance ($\Delta T/T$), we can observe the intricate correlation processes among the charge, lattice, and spin degrees of freedom, which are explicitly recognized in different characteristic time scales. Thus, the microscopic mechanism of the magnetoelectric coupling or magnetoelastic behavior in this kind of strongly correlated materials can be revealed.

3. Electronic Structure Revealed by Optical Spectroscopy

To understand the extensive physical properties in multiferroic $ReMnO_3$ materials, it is crucial to realize the electronic band structure. With respect to the crystal structure of hexagonal $ReMnO_3$ manganites with MnO_5 bipyramids, in contrast with the MnO_6 octahedron of orthorhombic structure which split to t_{2g} and e_g, the crystal field symmetry leads the quintet d levels of Mn^{3+} ion splits into two low lying doublets of e_{2g} and e_{1g} (d_{xz}/d_{yz} and $d_{xy}/d_{x^2-y^2}$) states and one singlet a_{1g} ($d_{3z^2-r^2}$) state. In general, optical spectroscopy is one of the powerful tools for investigating the electronic band structure in materials. Therefore, this structural difference between the hexagonal and orthorhombic phases could be disclosed by the optical spectra [60, 61].

3.1. Linear Optical Absorption Spectra. The first optical measurements in hexagonal $YMnO_3$ were performed by Kritayakirana et al. in 1969 [62], who observed that a near infrared absorption edge moves to higher energy with lowering temperature. For the case of hexagonal $ScMnO_3$ and $ErMnO_3$, the spectra of the real and imaginary parts of the dielectric function were also measured by Kalashnikova and Pisarev [63]. An abnormally drastic absorption peak in the region of 1.57–1.59 eV is the most pronounced feature in the dielectric spectra. This peak exhibits asymmetry and can be decomposed into two components by peak fitting with the Gaussian functions. Furthermore, the absorption intensity in the region above 2.2–2.4 eV increases with photon energy. In addition, hexagonal $HoMnO_3$ [64] and $LuMnO_3$ [31] also exhibit similar results. It is noteworthy that the near infrared absorption peak exhibits a substantial blueshift of ~0.16 eV from 300 K to 10 K as shown in Figure 3. Recently, Choi et al. [32] reported a systematic study on the hexagonal $ReMnO_3$ (R = Gd, Tb, Dy, and Ho), and the overall features in the spectra are similar to previous results. The most surprising part of those results is that the temperature-dependent absorption peak at ~1.7 eV shows an unexpectedly large blueshift near T_N among the rare-earth ions of Re = Lu, Gd, Tb, Dy, and Ho, as shown in Figure 4(a).

The assignment of the optical absorption peak at ~1.7 eV has also been an issue. One interpretation is that it comes from the charge transfer transition from the O 2p to the Mn 3d states [30, 63, 65, 66]. The photoemission spectroscopy (PES) study proposed that the O 2p is the highest occupied state, while the Mn $d_{3z^2-r^2}$ state is mostly unoccupied. Other occupied Mn 3d states (d_{xz}/d_{yz}, and $d_{xy}/d_{x^2-y^2}$) lie deep below E_F [65]. The result of the first-principle electronic structure calculations also suggested that the top of the valence band is mainly determined by the O 2p states, and the lowest unoccupied band is formed by the $d_{3z^2-r^2}$ of Mn [30, 66]. The other interpretation, which is also an extensively convincing explanation, is that it comes from on-site d-d transition between the Mn 3d levels [31, 34, 64, 67]. The transition was attributed to the d-d transition between occupied e_{2g} and e_{1g} (d_{xz}/d_{yz}, and $d_{xy}/d_{x^2-y^2}$) orbitals and the unoccupied a_{1g} ($d_{3z^2-r^2}$) orbit, as shown in Figure 4(b). Because of the selection rule, transitions between d orbitals are forbidden. However, the selection rule is relaxed through the strong hybridization between the O 2p bands and transition metal d bands, which was observed in the hexagonal phase but not in the orthorhombic phase [60]. Furthermore, the strong peak at ~5 eV is attributed to the charge transfer transition from the hybridized O 2p level to the Mn $d_{3z^2-r^2}$ level.

The other feature of the near infrared absorption peak is that it shows the blueshift as decreasing temperatures accompanying the dramatic changes near T_N, which indicates

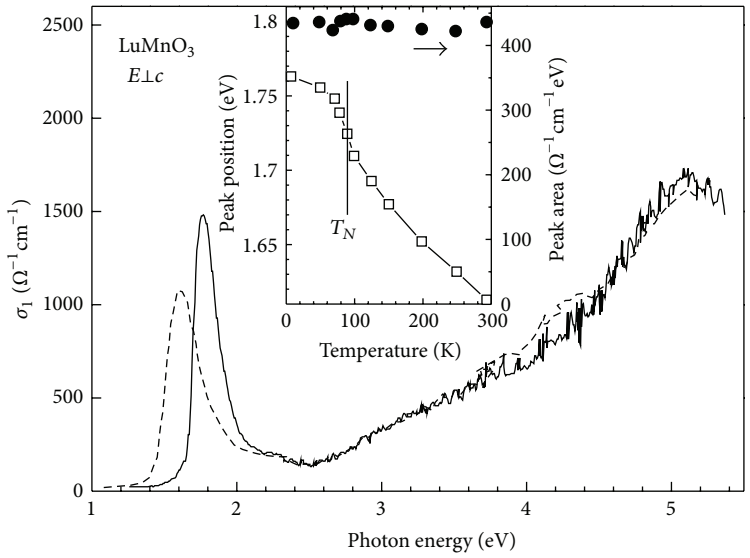

FIGURE 3: Electronic conductivity of $LuMnO_3$ at 300 K (dashed line) and 10 K (solid line). Inset: temperature-dependent peak position (open squares) and spectral weight (solid circles) of the absorption peak around 1.7 eV [31]. Reprinted figure with permission from Souchkov et al. [31]. Copyright (2003) by the American Physical Society.

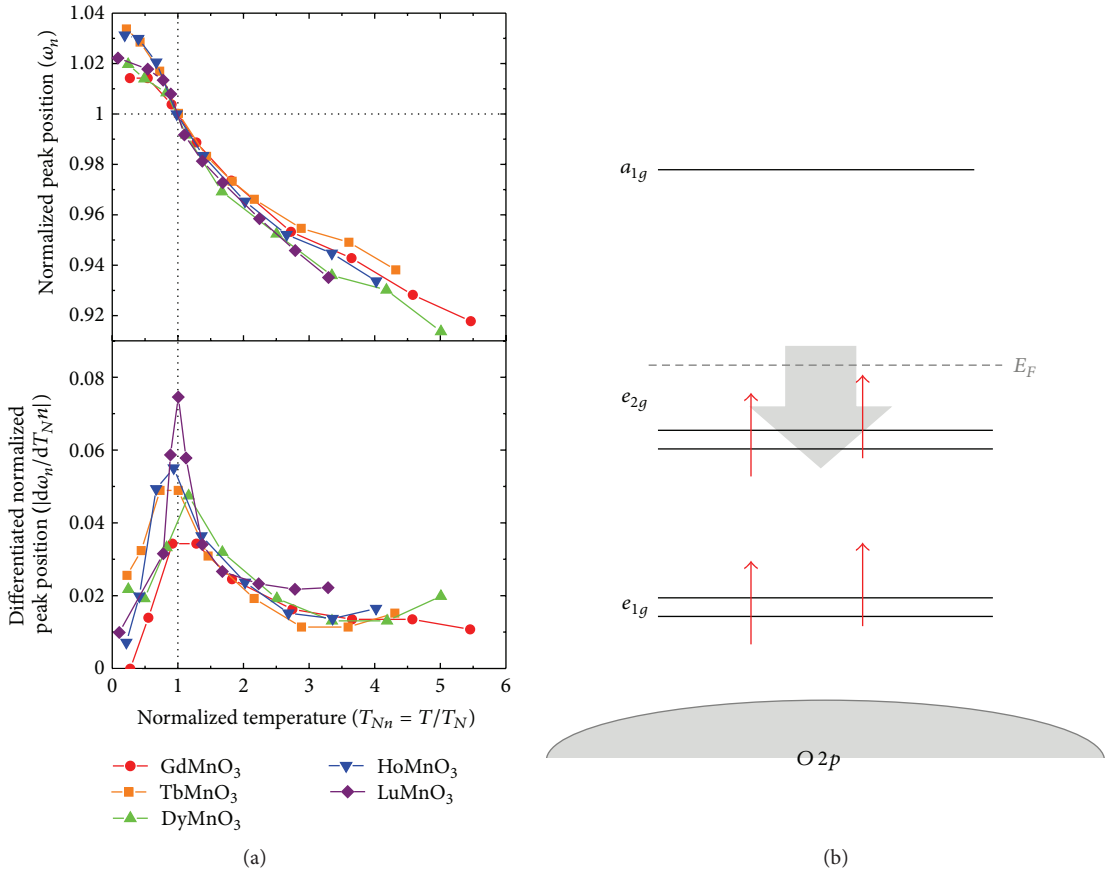

(a) (b)

FIGURE 4: (a) Upper panel: temperature dependence of the peak positions normalized to the peak position at T_N as a function of the normalized temperature T_{Nn} ($\equiv T/T_N$). Lower panel: absolute value of normalized peak position differentiated to normalized temperature [32]. Reprinted figure with permission from Choi et al. [32]. Copyright (2008) by the American Physical Society. (b) Schematic diagram of the d-d transition in $ReMnO_3$. The red arrows indicate electrons reside in the d orbitals, and the gray arrow indicates lowering of e_{2g} band caused by the temperature reduction.

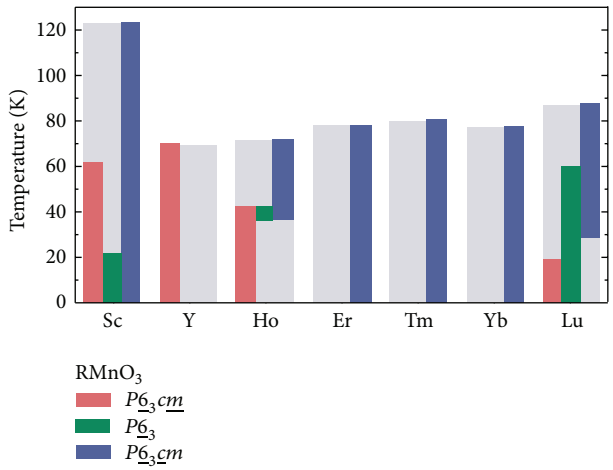

FIGURE 5: Magnetic symmetry of the hexagonal manganites. Sc, Ho, and Lu show a coexistence of magnetic phases with temperature intervals being sample specific. (Rare-earth spin ordering below 6 K was not considered) [33]. Reprinted figure with permission from Fiebig et al. [33]. Copyright (2000) by the American Physical Society.

the effective coupling between the electronic structure and the magnetic ordering. Souchkov et al. [31] attributed this temperature-dependent blueshift to the effects of exchange interactions between the Mn^{3+} ions. The superexchange between Mn^{3+} neighbors leads to lower $d_{xy}/d_{x^2-y^2}$ levels, whereas the $d_{3z^2-r^2}$ level is rarely affected (see Figure 4(b)). Moreover, together with the temperature-dependent and magnetic-dependent results [32] further implies that the magnetic ordering seriously influences the electronic structure.

3.2. Second Harmonic Generation Spectra. From the linear absorption spectra, the strong absorption caused by the d-d transition from e_{2g} to a_{1g} was clearly observed in hexagonal manganites. But the transition from e_{1g} to a_{1g} is another question. Recently, the second harmonic generation (SHG) was successfully used to explore the hidden localized d-d transitions, even those embedded in the much stronger absorption peaks [68]. The nonlinear polarization induced by optical waves is given by

$$\mathbf{P}_i(2\omega) = \varepsilon_0 \left(\chi_{ijk}^{(i)} + \chi_{ijk}^{(c)}\right) \mathbf{E}_j(\omega)\, \mathbf{E}_k(\omega), \quad (1)$$

where $\mathbf{P}_i(2\omega)$ is the nonlinear polarization induced in a medium. $\mathbf{E}_j(\omega)$ and $\mathbf{E}_k(\omega)$ are the electric field components of the fundamental light. $\chi_{ijk}^{(i)}$ and $\chi_{ijk}^{(c)}$ are the second-order nonlinear susceptibility tensor which are uniquely defined by the crystalline and magnetic structure of the crystal, respectively. The subscripts i, j, and k correspond to the Cartesian coordinate axes x, y, and z. i is the direction of the nonlinear polarization generated; j and k are the directions of applied optical field.

There are two types of optical SHG in multiferroic hexagonal manganites. One is caused by the noncentrosymmetric ferroelectric ordering of charges and the nonlinear susceptibility is time invariant (i-type). The other is due to the centrosymmetric antiferromagnetic ordering of spins and the susceptibility is time noninvariant (c-type) [34]. Table 1 lists the allowed susceptibility tensor components in i-type and c-type. Thus, the SHG contribution from ferroelectric and antiferromagnetic can be distinguished easily. Figure 5 summarizes the magnetic symmetries of all the hexagonal $ReMnO_3$ compounds as derived from the SHG experiments [33].

TABLE 1: Nonvanished susceptibility tensor components for hexagonal $ReMnO_3$ with antiparallel coupling of corresponding Mn^{3+} spins along the z-axis.

	Space group	Tensor components χ_{ijk}
Nonmagnetic SH (i-type)	$P6_3cm$	$xxz = xzx = yyz = yzy$, $zxx = zyy$, zzz
Magnetic SH (c-type)	$P6_3\underline{c}\underline{m}$	$yxx = xyx = xxy = -yyy$
	$P6_3\underline{c}m$	$xyy = yxy = yyx = -xxx$
	$P6_3$	sum of $P6_3\underline{c}\underline{m}$ and $P6_3\underline{c}m$

The polarization $\mathbf{P}^{\mathrm{FE}}(2\omega)$ with the space group $P6_3cm$ below the Curie temperature T_C is

$$\begin{aligned} \mathbf{P}_x^{\mathrm{FE}}(2\omega) &= 2\varepsilon_0 \chi_{xxz}^{(i)} \mathbf{E}_x(\omega)\, \mathbf{E}_z(\omega), \\ \mathbf{P}_y^{\mathrm{FE}}(2\omega) &= 2\varepsilon_0 \chi_{xxz}^{(i)} \mathbf{E}_y(\omega)\, \mathbf{E}_z(\omega), \\ \mathbf{P}_z^{\mathrm{FE}}(2\omega) &= \varepsilon_0 \chi_{zxx}^{(i)} \left[\mathbf{E}_x^2(\omega) + \mathbf{E}_y^2(\omega)\right] + \varepsilon_0 \chi_{zzz}^{(i)} \mathbf{E}_z^2(\omega). \end{aligned} \quad (2)$$

The contribution from antiferromagnetic $\mathbf{P}^{\mathrm{AFM}}(2\omega)$ below T_N for the space group $P6_3\underline{c}\underline{m}$ (e.g., $YMnO_3$ [68, 69]) is

$$\begin{aligned} \mathbf{P}_x^{\mathrm{AFM}}(2\omega) &= 2\varepsilon_0 \chi_{yyy}^{(c)} \mathbf{E}_x(\omega)\, \mathbf{E}_y(\omega), \\ \mathbf{P}_y^{\mathrm{AFM}}(2\omega) &= \varepsilon_0 \chi_{yyy}^{(c)} \left[\mathbf{E}_x^2(\omega) - \mathbf{E}_y^2(\omega)\right], \\ \mathbf{P}_z^{\mathrm{AFM}}(2\omega) &= 0. \end{aligned} \quad (3)$$

Figure 6(a) exhibits the SHG spectra of zxx component in $YMnO_3$ at 6 K [34]. The strong peak is centered at 2.7 eV, which could be assigned to $^5\Gamma_2(^5\Gamma_6) \rightarrow {}^5\Gamma_1\,(^5\Gamma_1)$ (corresponds to $e_{1g} \rightarrow a_{1g}$) transition. Figure 6(b) right panel shows the spectrum of χ_{yyy}. Peaks at 2.46 eV represent the $^5\Gamma_1(^5\Gamma_6) \rightarrow {}^5\Gamma_1\,(^5\Gamma_1)$ (corresponds to $e_{1g} \rightarrow a_{1g}$) transition. These assignments have been proved by several studies [47, 68, 69]. In the inset of Figure 6(b), the temperature-dependent intensity of 2.46 eV disappears once the temperature is higher than T_N, which strongly indicates the closed correlation between the antiferromagnetic order parameter and SHG.

Consequently, the electronic structure of hexagonal manganites has been clearly depicted by linear and nonlinear optical spectroscopy, which further provides the basis for the excitation and relaxation of electrons in pump-probe spectroscopy.

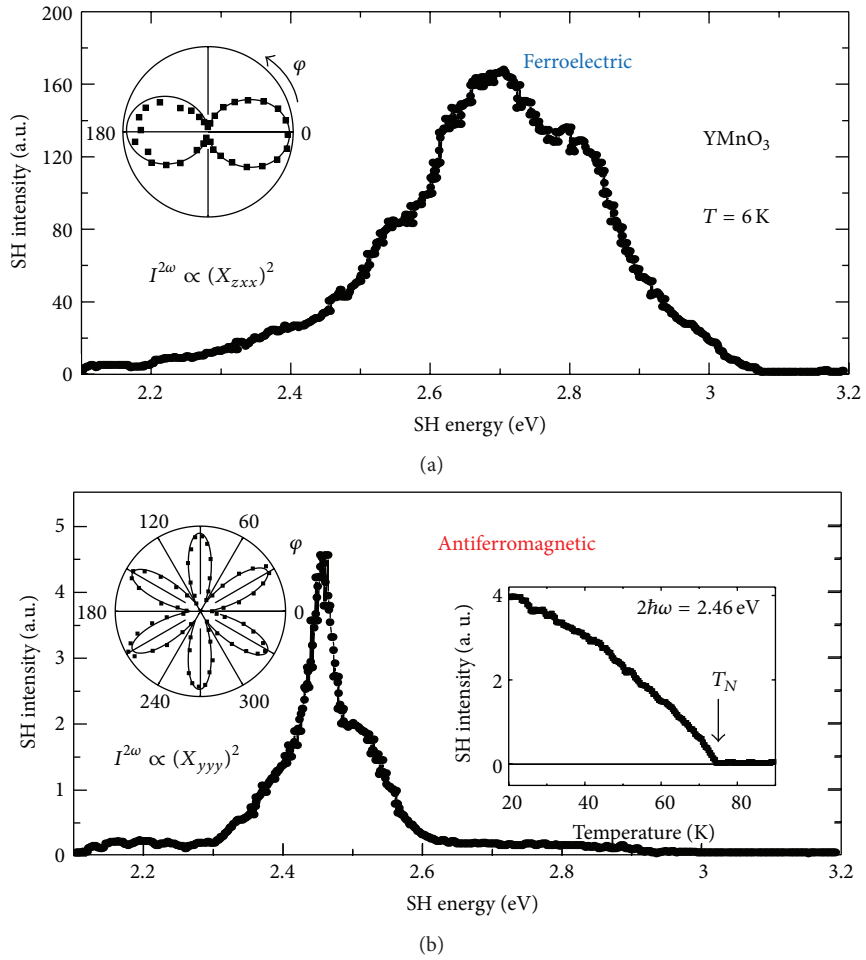

Figure 6: SHG spectra of $YMnO_3$ due to (a) the ferroelectric ordering and (b) antiferromagnetic ordering; inset: temperature dependence of the SHG intensity of 2.46 eV [34]. Reprinted figure with permission from Fröhlich et al. [34]. Copyright (1998) by the American Physical Society.

4. Ultrafast Pump-Probe Spectroscopy

Ultrafast optical pump-probe spectroscopy has proven to be a powerful tool to investigate the dynamics of electron-electron interaction, electron-phonon interaction, and electron-spin interaction in various materials (see, e.g., [70–72]). To understand the underlying mechanisms in strongly correlated materials, the interactions between these order parameters should be derived first. Because of the different characteristic time scales and characteristic behavior for various degrees of freedom existing in these complex materials, ultrafast spectroscopy can determine the coupling between each order of parameters.

As shown in Figure 7, the general idea of the pump-probe technique is that changes of a sample induced by a pump pulse are obtained by detecting the change in the reflectivity (ΔR) or transmissivity (ΔT) of probe pulses as a function of probe delay time. The femtosecond time evolutions are derived by delaying the relative arrival time between the pump and probe pulses using a mechanical delay line. The fluence of a probe pulse is usually much weaker than that of a pump pulse in order to avoid second excitation in the samples. The polarizations of pump and probe pulses are set perpendicular to avoid interference between pump and probe beams [73].

Generally, this pump-probe spectroscopy composes two kinds of signals of the decay background and the oscillation, which relates to the relaxation of carriers and the dynamics of phonons or spins, respectively. By the Fourier transform, the frequency of phonon modes can be doubly obtained from the oscillation signals in pump-probe spectroscopy. Moreover, the phonon dynamics, that is, the time-evolution of oscillation signals, can be revealed by short-time Fourier transform (STFT), which cannot be reached by common Raman spectroscopy. Thus, the pump-probe spectroscopy is a powerful tool to provide the information in time- and frequency-domain simultaneously.

4.1. Spin-Charge Coupling. Since the magnetic ordering and the electronic structure of manganites are strongly correlated, as found in temperature-dependent absorption spectra, there is a strong coupling between charge and spin, which can be revealed by the time-resolved femtosecond spectroscopy

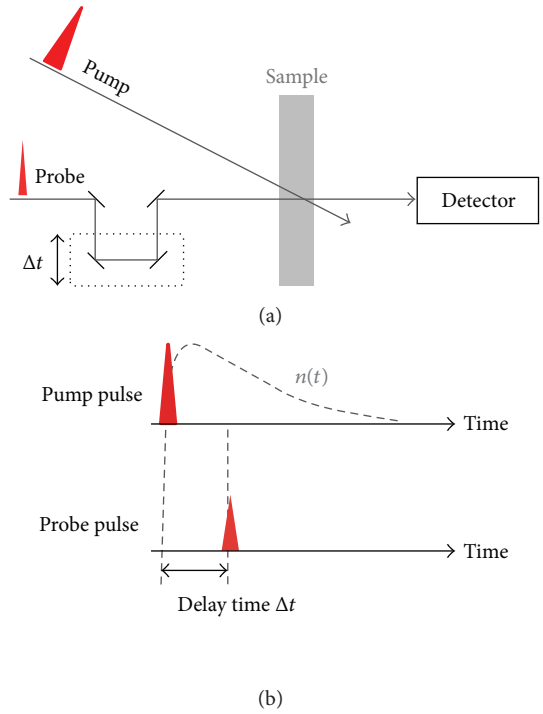

FIGURE 7: (a) Schematic diagram of pump-probe technique. Time delay (Δt) between pump and probe pulses can be controlled by a mechanical delay line. (b) The fundamental principle of pump-probe experiments. Time varying refractive index $n(t)$ changes of the sample induced by pump pulses were observed by detecting the intensity variations of probe pulses.

[72]. Shih et al. observed the spin-charge coupling by various photon energy excitations on hexagonal $HoMnO_3$ single crystals [35]. As shown in Figure 8(a), the $\Delta R/R$ amplitude as a function of temperature shows a significant drop to cross zero amplitude line to become negative at some characteristic temperatures. The excitation photon energy used in the experiment changes from 1.52 to 1.68 eV, which is exactly the range covering the d-d transition energy E_{dd} (transition from e_{2g} to a_{1g}) in the hexagonal $ReMnO_3$. When the photon energy is larger than E_{dd}, the electrons in the e_{2g} orbit can transfer to the unoccupied a_{1g} orbital by absorbing pumping photons. Conversely, this onsite transition would be completely blocked when the transition energy E_{dd} becomes larger than the pumping photon energy. Thus, the $\Delta R/R$ amplitude vanishes at a certain temperature T_0, which drops with increasing photon energy, indicating the blueshift of E_{dd}. Furthermore, Shih et al. found that the optical pump-probe measurement is sensitive to short-range magnetic order. In Figure 8(b), the E_{dd} as a function of T_0 demonstrates a gradual increase in the extent of antiferromagnetic (AFM) ordering. Moreover, this ordering starts to deviate from linearity around T_N (~76 K), suggesting the prevalence of global long-range AFM ordering. The AFM correlation evolves with temperature as it is close to T_N, shown as $d(\Delta R/R)_p/dT$ in Figure 8(c). Later, Wu et al. obtained similar results for hexagonal $YMnO_3$ thin films [74]. Furthermore, they found that the strain-induced changes of T_N, which are difficult to be observed by the temperature-dependent magnetization measurements, can be clearly revealed by the shift of $d(\Delta R/R)_p/dT$.

As a result, the amplitude of the initial rising component of $\Delta R/R$ corresponding to the Mn^{3+} d-d transition is caused by strong coupling between the electronic structure and magnetic ordering. Moreover, the emergence of long-range and short-range magnetic orders can be clearly observed by optical pump-probe spectroscopy.

4.2. Spin-Lattice Coupling. Optically induced lattice vibration can be observed through optical pump-probe spectroscopy through a periodic oscillation. This periodic oscillation in reflectivity (or transmissivity), so-called coherent acoustic phonons, is caused by interference between the reflected probe beams from sample surface and the wave front of the propagating strain pulse generated upon the pump pulse [75, 76]. On the other hand, vibration with frequencies corresponding to optical phonon modes in various materials has been observed by pump-probe spectroscopy. A number of mechanisms have been proposed to explain these oscillations, for example, the displacive excitation of coherent phonons (DECP) [77] and the impulsive stimulated Raman scattering (ISRS) [78, 79]. The simplest idea is that a pump pulse creates a standing wave which was generated by the coherent ionic motion. Then a following probe pulse senses the changes of refractive index which is modulated by the standing wave. In general, the reflectivity (or transmissivity) oscillation observed in pump-probe spectroscopy always corresponds to the optical phonon modes observed in Raman spectroscopy. In conclusion, the measurements of coherent acoustic or optical phonons dynamics at various temperatures are useful to study the spin-lattice coupling in multiferroic materials.

4.2.1. Coherent Optical Phonons. Figure 9 shows the reflectivity oscillation of ~3.6 THz (~120 cm^{-1}) in $LuMnO_3$ [36, 37]. According to Raman studies, this vibration mode can be attributed to optical phonon of A_1 symmetry [80–82]. This fully symmetric mode corresponds to the Lu1 and Lu2 atomic motions in opposite directions along the c-axis, as depicted in Figure 9(d) [36]. In temperature-dependent measurements, the optical phonon almost disappears below T_N, as shown in Figures 9(e) and 9(f) [37]. Additionally, the structural change from highly symmetry space group $P6_3/mmc$ to the tilted and distorted $P6_3cm$ ferroelectric structure [14] in hexagonal manganites (see Figure 1) takes place at the Curie temperature (T_C), which is much higher than T_N. Since there is no structural transition near T_N, the atomic motions of the optical phonon mode would be affected by the appearance of magnetic ordering. In other words, the disappearance of optical phonon mode might be attributed to the magneto-elastic coupling. In temperature-dependent Raman studies, the lowest frequency A_1 mode also shows anomaly at T_N in $YMnO_3$ [82], $ErMnO_3$ [83], and $LuMnO_3$ [80, 82] which support close relation between phonon and spin systems.

4.2.2. Coherent Acoustic Phonons. Coherent acoustic phonons have been observed in many kinds of hexagonal

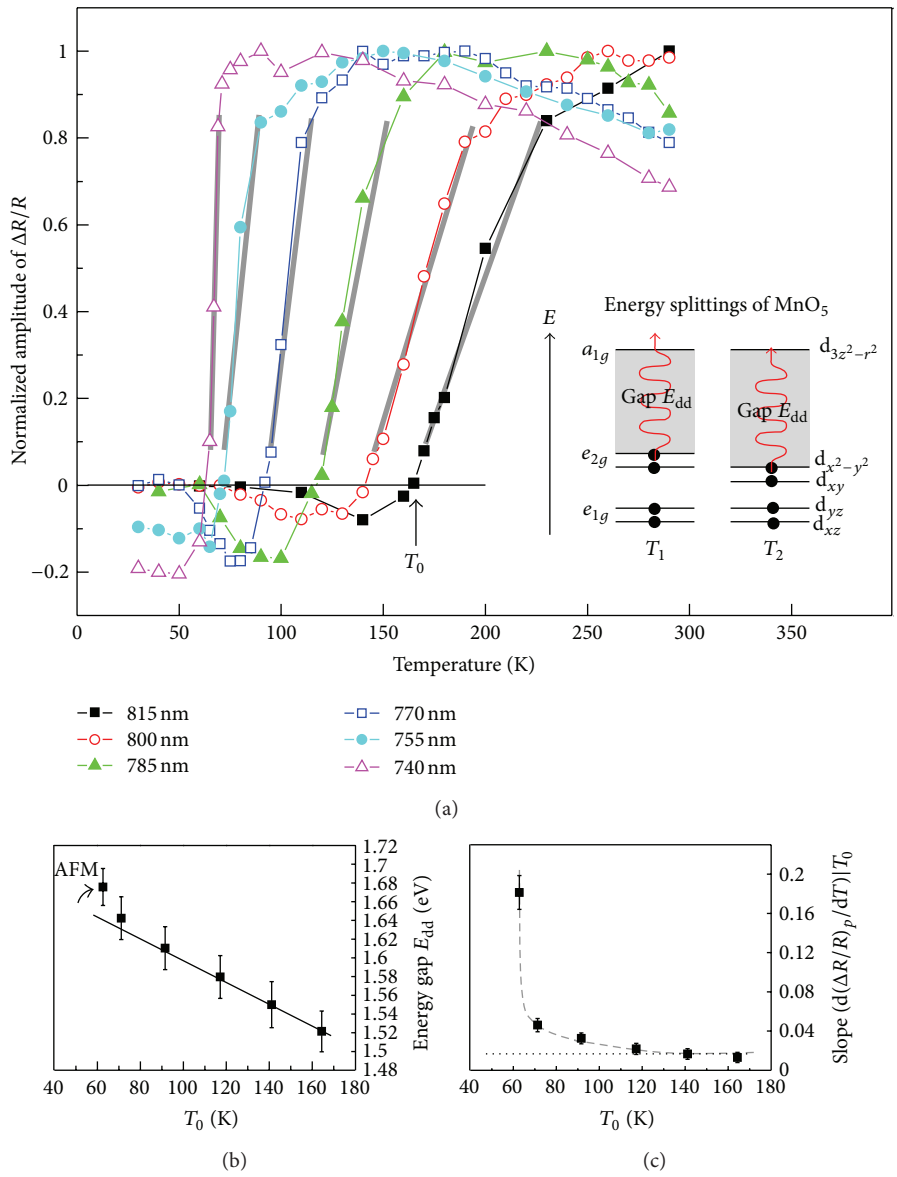

FIGURE 8: (a) Normalized amplitude of $\Delta R/R$ as a function of temperature at various wavelengths. The insets illustrate splitting of the Mn^{3+} energy levels in the local environment MnO_5 for photon energy above and below E_{dd} ($T_1 > T_2$). (b) Energy gap E_{dd} as a function of T_0. E_{dd} is estimated from the wavelengths in (a). The dashed line emphasizes linear behavior in the high-temperature range. (c) The slope of temperature-dependent normalized amplitude of $\Delta R/R$ in (a) (gray thick lines) as a function of T_0 at various wavelengths. The dashed line emphasizes behavior of the slope [35]. Reprinted figure with permission from Shih et al. [35]. Copyright (2009) by the American Physical Society.

manganites such as $LuMnO_3$ [37, 84], $YMnO_3$ [39], and $HoMnO_3$ [38]. The damped oscillation behavior in reflectivity changes with time delay t could be described as follows [76]:

$$\frac{\Delta R}{R} \propto \left(\frac{\Delta R}{R}\right)_0 \cos\left(\frac{4\pi n v_s}{\lambda} t - \phi\right) e^{-(v_s/\xi)t}, \quad (4)$$

where λ is the wavelength of the probe pulses, n is the refraction index of samples without strain, v_s is the strained layer propagating sound speed, and ξ is the penetration depth of probe pulses. The frequency of the oscillation is given as $\omega = 4\pi n v_s/\lambda$ and the dephasing time is ξ/v_s.

According to (4), the dephasing time is proportional to the penetration depth of probe pulses ξ and the inverse sound velocity $1/v_s$. However, the skin depth is much shorter than the propagating length of the strain pulse. Therefore, the dephasing time is dominated by the finite penetration depth ξ of the probe [84]. The dephasing time of acoustic phonons shows strong temperature dependence (Figure 10), and the anomalous increase of the dephasing time near T_N might be because of the photon energy being close to the edge of d-d transition. In other words, the penetration depth increases and the absorption of probe photons for the d-d

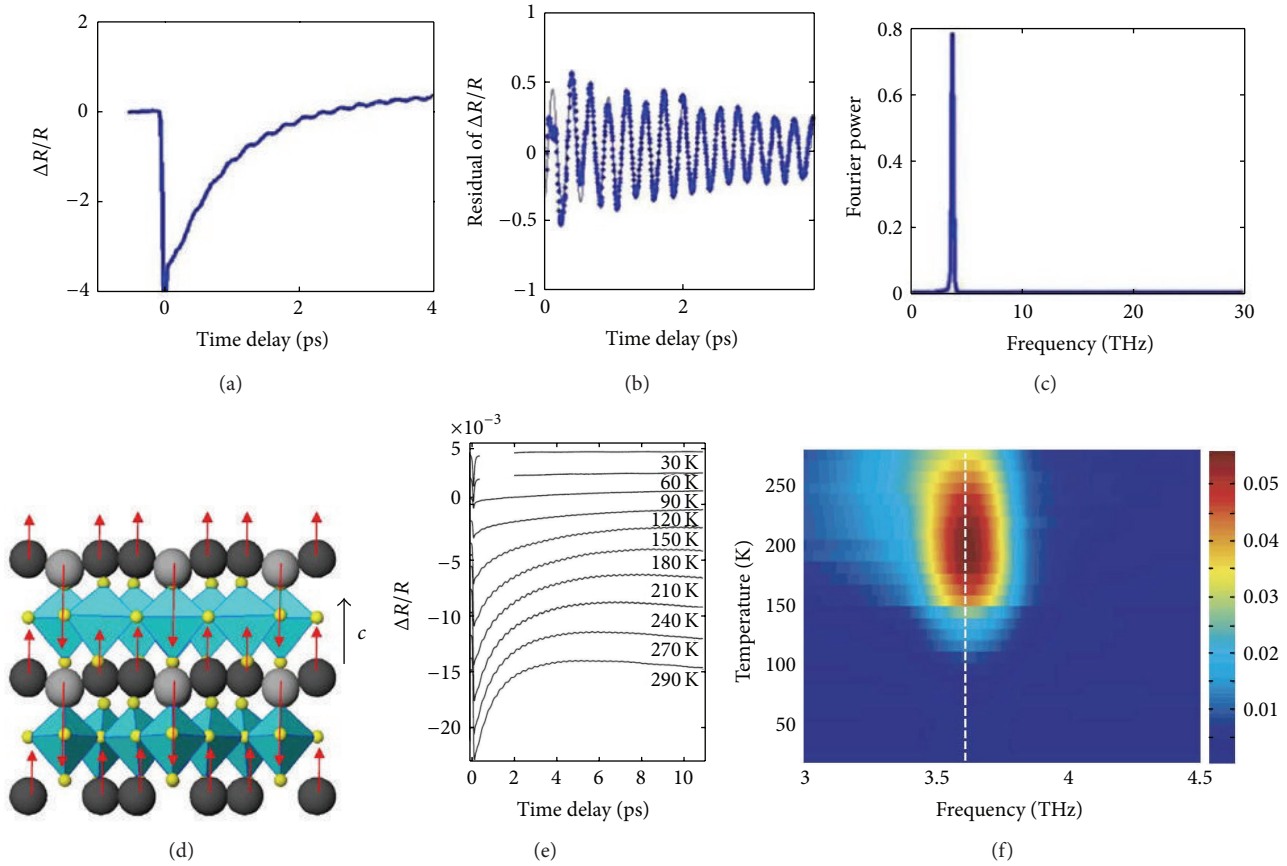

FIGURE 9: $LuMnO_3$ measured at 293 K. (a) $\Delta R/R$ as a function of time delay. (b) Oscillation component after subtraction of the slowly varying response. (c) Fourier power spectrum of the data with frequency 3.61 THz. (d) Schematic of the coherently excited A_1 phonon mode [36]. Reprinted figure with permission from Lou et al. [36]. Copyright (2009) by the American Physical Society. (e) $\Delta R/R$ at various temperatures. (f) Fourier transformed amplitudes of coherent optical phonon [37]. Figures were reproduced with permission from Jang et al. [37].

transition decreases (due to the blueshift of E_{dd} as mentioned in Section 3.1) as the temperature decreases.

The amplitude and period of the oscillation component in $\Delta R/R$ show strong temperature dependence as shown in Figure 11. Both of these parameters are clearly anomalous near the magnetic ordering temperature T_N. The amplitude of the oscillation component in $\Delta R/R$ gradually increases with decreasing temperature and reaches the maximum near a characteristic temperature (~190 K for $YMnO_3$ [39] and ~200 K for $LuMnO_3$ [37]). Then it decreases when the temperature approaches T_N, as shown in Figure 11(a). This may imply the appearance of AFM short-range ordering, as mentioned in [35]. On the other hand, the period of the oscillation component in $\Delta R/R$ also slightly shrinks with decreasing temperature. Surprisingly, it dramatically shrinks around T_N as shown in Figure 11(b). This strongly indicates the close correlation between AFM ordering and the propagation of thermal stress along c-axis, which is consistent with the results in heat capacity measurements [13, 85]. In addition, the ferroelectric polarization along the c-axis caused by polyhedron tilting of MnO_5 and distortion of the rare-earth ions [14] is well known. Thus, the propagation of a strain pulse with the modulation of dielectric constant (or ferroelectric polarization) along c-axis is indeed affected by the appearance of AFM ordering. Neutron diffraction experiments also have demonstrated the extra displacement of the rare-earth and oxygen atoms along c-axis at T_N [52]. Finally, these results in amplitude and period of the oscillation component in $\Delta R/R$ provide evidence for magnetoelastic coupling in these intriguing materials.

5. Summary and Outlook

In this paper, the recent developments on the electronic structures and ultrafast dynamics of hexagonal manganites have been reviewed. The electronic structure can be clearly revealed by the static linear optical absorption spectra and nonlinear second harmonic generation spectra. The temperature-dependent d-d transition energy exhibits an unexpected change near the spin ordering temperature T_N. This strongly indicates the coupling between electronic structure and antiferromagnetism in hexagonal manganites. Fortunately, the photon energy of the pulse laser used in pump-probe spectroscopy accidentally fits well the d-d transition (from e_{2g} to a_{1g}) energy. Therefore, the pump-probe

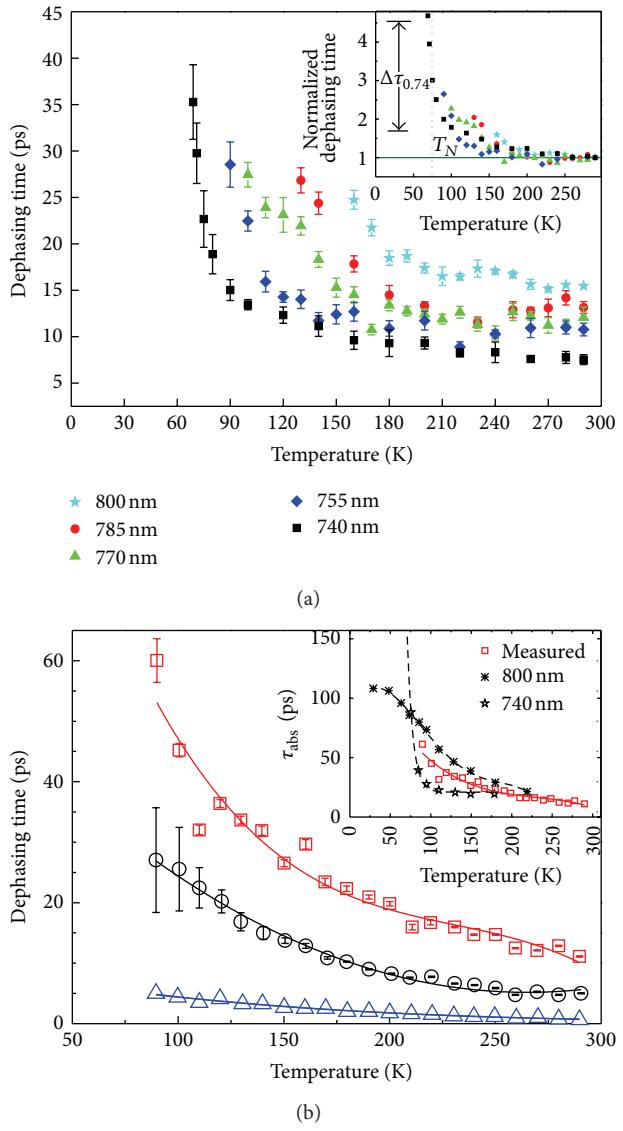

FIGURE 10: (a) Temperature dependence dephasing time of the oscillation component in $\Delta R/R$ at various wavelengths of $HoMnO_3$. Inset: the normalized dephasing time as a function of temperatures at various wavelengths [38]. Figures were reproduced with permission from Shih et al. [38]. (b) Temperature dependence of dephasing times: red squares for acoustic phonons, black circles for optical phonons, and blue triangles for electronic relaxation time [37]. Figures were reproduced with permission from Jang et al. [37].

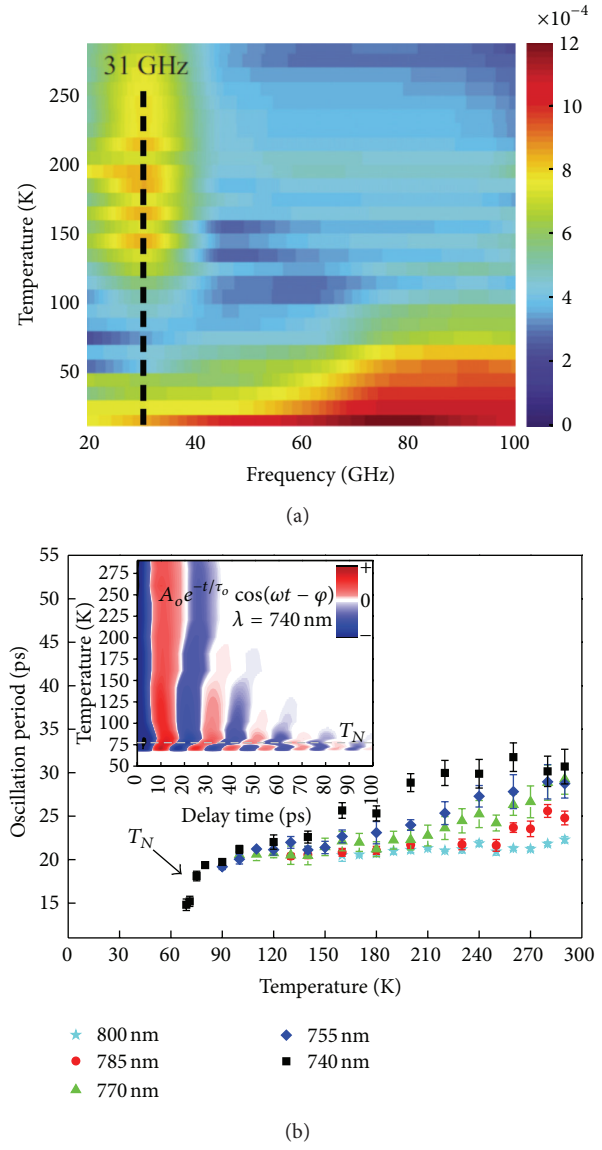

FIGURE 11: (a) Fourier transform amplitudes for coherent oscillation of $YMnO_3$ [39]. Reprinted with permission from Jang et al. [39]. Copyright 2010, American Institute of Physics. (b) Temperature dependence oscillation period in $\Delta R/R$ at various wavelengths of $HoMnO_3$. Inset: the evolution of the oscillation component in $\Delta R/R$ at various temperatures [38]. Figures were reproduced with permission from Shih et al. [38].

measurements can reveal the ultrafast dynamics through the spin-charge coupling and spin-phonon coupling.

However, those ultrafast dynamic experiments only present the charge dynamics between e_{2g} and a_{1g}. If the laser spectrum could cover the whole range of d-d transition, that is, containing the transition from e_{1g} to a_{1g} and e_{2g} to a_{1g}, it could disclose all of the charge dynamics in these strongly magnetic influenced d orbitals. The optical parametric amplifier (OPA) is a suitable light source for this kind of study. Consequently, if all of the charge dynamics in the d orbitals could be completely revealed, it would shed light on the microscopic mechanism of the magnetoelectric coupling or magnetoelastic effect in this kind of strongly correlated material.

Acknowledgments

This work was supported by the National Science Council of Taiwan, under Grants nos. NSC98-2112-M-009-008-MY3, NSC101-2112-M-009-016-MY2 and by the MOEATU Program at NCTU of Taiwan, Taiwan.

References

[1] M. Fiebig, "Revival of the magnetoelectric effect," *Journal of Physics D*, vol. 38, no. 8, pp. R123–R152, 2005.

[2] D. I. Khomskii, "Multiferroics: different ways to combine magnetism and ferroelectricity," *Journal of Magnetism and Magnetic Materials*, vol. 306, no. 1, pp. 1–8, 2006.

[3] W. Eerenstein, N. D. Mathur, and J. F. Scott, "Multiferroic and magnetoelectric materials," *Nature*, vol. 442, no. 7104, pp. 759–765, 2006.

[4] C. W. Nan, M. I. Bichurin, S. Dong, D. Viehland, and G. Srinivasan, "Multiferroic magnetoelectric composites: historical perspective, status, and future directions," *Journal of Applied Physics*, vol. 103, no. 3, Article ID 031101, 2008.

[5] T. Lottermoser, T. Lonkai, U. Amann, D. Hohlwein, J. Ihringer, and M. Fiebig, "Magnetic phase control by an electric field," *Nature*, vol. 430, no. 6999, pp. 541–544, 2004.

[6] B. Lorenz, Y. Q. Wang, and C. W. Chu, "Ferroelectricity in perovskite $HoMnO_3$ and $YMnO_3$," *Physical Review B*, vol. 76, no. 10, Article ID 104405, 2007.

[7] B. Lorenz, Y. Q. Wang, Y. Y. Sun, and C. W. Chu, "Large magnetodielectric effects in orthorhombic $HoMnO_3$ and $YMnO_3$," *Physical Review B*, vol. 70, no. 21, Article ID 212412, 2004.

[8] T. Kimura, T. Goto, H. Shintani, K. Ishizaka, T. Arima, and Y. Tokura, "Magnetic control of ferroelectric polarization," *Nature*, vol. 426, no. 6962, pp. 55–58, 2003.

[9] M. Fiebig, T. Lottermoser, D. Fröhlich, A. V. Goltsev, and R. V. Pisarev, "Observation of coupled magnetic and electric domains," *Nature*, vol. 419, no. 6909, pp. 818–820, 2002.

[10] N. Hur, S. Park, P. A. Sharma, J. S. Ahn, S. Guha, and S. W. Cheong, "Electric polarization reversal and memory in a multiferroic material induced by magnetic fields," *Nature*, vol. 429, no. 6990, pp. 392–395, 2004.

[11] W. Prellier, M. P. Singh, and P. Murugavel, "The single-phase multiferroic oxides: from bulk to thin film," *Journal of Physics*, vol. 17, no. 30, pp. R803–R832, 2005.

[12] S. W. Cheong and M. Mostovoy, "Multiferroics: a magnetic twist for ferroelectricity," *Nature Materials*, vol. 6, no. 1, pp. 13–20, 2007.

[13] T. Katsufuji, S. Mori, M. Masaki, Y. Moritomo, N. Yamamoto, and H. Takagi, "Dielectric and magnetic anomalies and spin frustration in hexagonal $RMnO_3$ (R = Y, Yb, and Lu)," *Physical Review B*, vol. 64, no. 10, Article ID 104419, 2001.

[14] B. B. Van Aken, T. T. M. Palstra, A. Filippetti, and N. A. Spaldin, "The origin of ferroelectricity in magnetoelectric $YMnO_3$," *Nature Materials*, vol. 3, no. 3, pp. 164–170, 2004.

[15] C. J. Fennie and K. M. Rabe, "Ferroelectric transition in $YMnO_3$ from first principles," *Physical Review B*, vol. 72, no. 10, Article ID 100103, 2005.

[16] T. H. Lin, C. C. Hsieh, H. C. Shih et al., "Anomalous magnetic ordering in b-axis-oriented orthorhombic $HoMnO_3$ thin films," *Applied Physics Letters*, vol. 92, no. 13, Article ID 132503, 2008.

[17] M. N. Iliev, M. V. Abrashev, H. G. Lee et al., "Raman spectroscopy of orthorhombic perovskitelike $YMnO_3$ and $LaMnO_3$," *Physical Review B*, vol. 57, no. 5, pp. 2872–2877, 1998.

[18] J. S. Zhou and J. B. Goodenough, "Unusual evolution of the magnetic interactions versus structural distortions in $RMnO_3$ perovskites," *Physical Review Letters*, vol. 96, no. 24, Article ID 247202, 2006.

[19] W. C. Yi, C. S. Seo, S. I. Kwun, and J. G. Yoon, "Temperature dependence of capacitance/current-voltage characteristics of highly (0001)-oriented $YMnO_3$ thin films on Si," *Applied Physics Letters*, vol. 77, no. 7, pp. 1044–1046, 2000.

[20] H. N. Lee, Y. T. Kim, and S. H. Choh, "Comparison of memory effect between $YMnO_3$ and $SrBi_2Ta_2O_9$ ferroelectric thin films deposited on Si substrates," *Applied Physics Letters*, vol. 76, no. 8, pp. 1066–1068, 2000.

[21] S. Imada, T. Kuraoka, E. Tokumitsu, and H. Ishiwara, "Ferroelectricity of $YMnO_3$ thin films on $Pt(111)/Al_2O_3(0001)$ and $Pt(111)/Y_2O_3(111)/Si(111)$ structures grown by molecular beam epitaxy," *Japanese Journal of Applied Physics*, vol. 40, no. 2 A, pp. 666–671, 2001.

[22] Y. T. Kim, I. S. Kim, S. I. Kim, D. C. Yoo, and J. Y. Lee, "Atomic structure of random and c-axis oriented $YMnO_3$ thin films deposited on Si and Y_2O_3/Si substrates," *Journal of Applied Physics*, vol. 94, no. 8, pp. 4859–4862, 2003.

[23] T. Yoshimura, N. Fujimura, and T. Ito, "Ferroelectric properties of c-oriented $YMnO_3$ films deposited on Si substrates," *Applied Physics Letters*, vol. 73, no. 3, pp. 414–416, 1998.

[24] T. Lonkai, D. G. Tomuta, U. Amann et al., "Development of the high-temperature phase of hexagonal manganites," *Physical Review B*, vol. 69, no. 13, Article ID 134108, 2004.

[25] N. Fujimura, T. Ishida, T. Yoshimura, and T. Ito, "Epitaxially grown $YMnO_3$ film: new candidate for nonvolatile memory devices," *Applied Physics Letters*, vol. 69, no. 7, pp. 1011–1013, 1996.

[26] T. Kimura, S. Ishihara, H. Shintani et al., "Distorted perovskite with eg1 configuration as a frustrated spin system," *Physical Review B*, vol. 68, no. 6, Article ID 060403, 2003.

[27] T. Goto, T. Kimura, G. Lawes, A. P. Ramirez, and Y. Tokura, "Ferroelectricity and giant magnetocapacitance in perovskite rare-earth manganites," *Physical Review Letters*, vol. 92, no. 25, Article ID 257201, 2004.

[28] M. Tachibana, T. Shimoyama, H. Kawaji, T. Atake, and E. Takayama-Muromachi, "Jahn-Teller distortion and magnetic transitions in perovskite $RMnO_3$(R = Ho, Er, Tm, Yb, and Lu)," *Physical Review B*, vol. 75, no. 14, Article ID 14425, 2007.

[29] N. Iwata and K. Kohn, "Dielectric anomalies at magnetic transitions of hexagonal rare earth manganese oxides $RMnO_3$," *Journal of the Physical Society of Japan*, vol. 67, no. 9, pp. 3318–3319, 1998.

[30] J. E. Medvedeva, V. I. Anisimov, M. A. Korotin, O. N. Mryasov, and A. J. Freeman, "Effect of Coulomb correlation and magnetic ordering on the electronic structure of two hexagonal phases of ferroelectromagnetic $YMnO_3$," *Journal of Physics Condensed Matter*, vol. 12, no. 23, pp. 4947–4958, 2000.

[31] A. B. Souchkov, J. R. Simpson, M. Quijada et al., "Exchange interaction effects on the optical properties of $LuMnO_3$," *Physical Review Letters*, vol. 91, no. 2, Article ID 027203, 2003.

[32] W. S. Choi, S. J. Moon, S. S. A. Seo et al., "Optical spectroscopic investigation on the coupling of electronic and magnetic structure in multiferroic hexagonal $RMnO_3$ (R = Gd, Tb, Dy, and Ho) thin films," *Physical Review B*, vol. 78, no. 5, Article ID 054440, 2008.

[33] M. Fiebig, D. Fröhlich, K. Kohn et al., "Determination of the magnetic symmetry of hexagonal manganites by second harmonic generation," *Physical Review Letters*, vol. 84, no. 24, pp. 5620–5623, 2000.

[34] D. Fröhlich, S. Leute, V. V. Pavlov, and R. V. Pisarev, "Nonlinear optical spectroscopy of the two-order-parameter compound $YMnO_3$," *Physical Review Letters*, vol. 81, no. 15, pp. 3239–3242, 1998.

[35] H. C. Shih, T. H. Lin, C. W. Luo et al., "Magnetization dynamics and the Mn^{3+} *d-d* excitation of hexagonal $HoMnO_3$ single crystals using wavelength-tunable time-resolved femtosecond spectroscopy," *Physical Review B*, vol. 80, no. 2, Article ID 024427, 2009.

[36] S. T. Lou, F. M. Zimmermann, R. A. Bartynski, N. Hur, and S. W. Cheong, "Femtosecond laser excitation of coherent optical phonons in ferroelectric $LuMnO_3$," *Physical Review B*, vol. 79, no. 21, Article ID 214301, 2009.

[37] K. J. Jang, J. Lim, J. Ahn et al., "Ultrafast IR spectroscopic study of coherent phonons and dynamic spin-lattice coupling in multiferroic $LuMnO_3$," *New Journal of Physics*, vol. 12, no. 2, Article ID 023017, 2010.

[38] H. C. Shih, L. Y. Chen, C. W. Luo et al., "Ultrafast thermoelastic dynamics of $HoMnO_3$ single crystals derived from femtosecond optical pump-probe spectroscopy," *New Journal of Physics*, vol. 13, no. 5, Article ID 053003, 2011.

[39] K. J. Jang, H. G. Lee, S. Lee et al., "Strong spin-lattice coupling in multiferroic hexagonal manganite $YMnO_3$ probed by ultrafast optical spectroscopy," *Applied Physics Letters*, vol. 97, no. 3, Article ID 031914, 2010.

[40] B. G. Ueland, J. W. Lynn, M. Laver, Y. J. Choi, and S. W. Cheong, "Origin of electric-field-induced magnetization in multiferroic $HoMnO_3$," *Physical Review Letters*, vol. 104, no. 14, Article ID 147204, 2010.

[41] M. Fiebig, C. Degenhardt, and R. V. Pisarev, "Interaction of frustrated magnetic sublattices in $ErMnO_3$," *Physical Review Letters*, vol. 88, no. 2, Article ID 027203, 2002.

[42] O. P. Vajk, M. Kenzelmann, J. W. Lynn, S. B. Kim, and S. W. Cheong, "Magnetic order and spin dynamics in ferroelectric $HoMnO_3$," *Physical Review Letters*, vol. 94, no. 8, Article ID 087601, 2005.

[43] H. Lueken, "A magnetoelectric effect in $YMnO_3$ and $HoMnO_3$," *Angewandte Chemie*, vol. 47, no. 45, pp. 8562–8564, 2008.

[44] D. Khomskii, "Classifying multiferroics: mechanisms and effects," *Physics*, vol. 2 , article 20, 2009.

[45] A. Muñoz, J. A. Alonso, M. J. Martínez-Lope, M. T. Casáis, J. L. Martínez, and M. T. Fernández-Díaz, "Magnetic structure of hexagonal $RMnO_3$ (R = Y, Sc): thermal evolution from neutron powder diffraction data," *Physical Review B*, vol. 62, no. 14, pp. 9498–9510, 2000.

[46] A. Muñoz, J. A. Alonso, M. J. Martínez-Lope, M. T. Casáis, J. L. Martínez, and M. T. Fernández-Díaz, "Evolution of the magnetic structure of hexagonal $HoMnO_3$ from neutron powder diffraction data," *Chemistry of Materials*, vol. 13, no. 5, pp. 1497–1505, 2001.

[47] M. Fiebig, C. Degenhardt, and R. V. Pisarev, "Magnetic phase diagram of $HoMnO_3$," *Journal of Applied Physics*, vol. 91, no. 10, pp. 8867–8869, 2002.

[48] T. Lonkai, D. G. Tomuta, J. U. Hoffmann, R. Schneider, D. Hohlwein, and J. Ihringer, "Magnetic two-dimensional short-range order in hexagonal manganites," *Journal of Applied Physics*, vol. 93, no. 10, pp. 8191–8193, 2003.

[49] Z. J. Huang, Y. Cao, Y. Y. Sun, Y. Y. Xue, and C. W. Chu, "Coupling between the ferroelectric and antiferromagnetic orders in $YMnO_3$," *Physical Review B*, vol. 56, no. 5, pp. 2623–2626, 1997.

[50] D. G. Tomuta, S. Ramakrishnan, G. J. Niewenhuys, and J. A. Mydosh, "The magnetic susceptibility, specific heat and dielectric constant of hexagonal $YMnO_3$, $LuMnO_3$ and $ScMnO_3$," *Journal of Physics Condensed Matter*, vol. 13, no. 20, pp. 4543–4552, 2001.

[51] C. Dela Cruz, F. Yen, B. Lorenz et al., "Strong spin-lattice coupling in multiferroic $HoMnO_3$: thermal expansion anomalies and pressure effect," *Physical Review B*, vol. 71, no. 6, Article ID 060407(R), 2005.

[52] S. Lee, A. Pirogov, M. Kang et al., "Giant magneto-elastic coupling in multiferroic hexagonal manganites," *Nature*, vol. 451, no. 7180, pp. 805–809, 2008.

[53] D. Y. Cho, J. Y. Kim, B. G. Park et al., "Ferroelectricity driven by y d0-ness with rehybridization in $YMnO_3$," *Physical Review Letters*, vol. 98, no. 21, Article ID 217601, 2007.

[54] D. Talbayev, S. A. Trugman, A. V. Balatsky, T. Kimura, A. J. Taylor, and R. D. Averitt, "Detection of coherent magnons via ultrafast pump-probe reflectance spectroscopy in multiferroic $Ba_{0.6}Sr_{1.4}Zn_2Fe_{12}O_{22}$," *Physical Review Letters*, vol. 101, no. 9, Article ID 097603, 2008.

[55] A. V. Kimel, B. A. Ivanov, R. V. Pisarev, P. A. Usachev, A. Kirilyuk, and T. Rasing, "Inertia-driven spin switching in antiferromagnets," *Nature Physics*, vol. 5, no. 10, pp. 727–731, 2009.

[56] C. W. Luo, I. H. Wu, P. C. Cheng et al., "Quasiparticle dynamics and phonon softening in FeSe superconductors," *Physical Review Letters*, vol. 108, no. 25, Article ID 257006, 2012.

[57] C. W. Luo, I. H. Wu, P. C. Cheng et al., "Ultrafast dynamics and phonon softening in $Fe_{1+y}Se_{1-x}Te_x$ single crystals," *New Journal of Physics*, vol. 14, no. 10, Article ID 103053, 2012.

[58] A. V. Kimel, R. V. Pisarev, F. Bentivegna, and T. Rasing, "Time-resolved nonlinear optical spectroscopy of Mn^{3+} ions in rare-earth hexagonal manganites $RMnO_3$ (R = Sc, Y, Er)," *Physical Review B*, vol. 64, no. 20, Article ID 201103(R), 2001.

[59] A. V. Kimel, R. V. Pisarev, F. Bentivegna, and Th. Rasing, "Ultrafast optical spectroscopy of hexagonal manganites $RMnO_3$ (R = Y, Er, Sc)," *Ferroelectrics*, vol. 279, no. 1, pp. 135–176, 2002.

[60] W. C. Yi, S. I. Kwun, and J. G. Yoon, "Study on the electronic structure of hexagonal and orthorhombic $YMnO_3$," *Journal of the Physical Society of Japan*, vol. 69, no. 8, pp. 2706–2707, 2000.

[61] A. Filippetti and N. A. Hill, "Coexistence of magnetism and ferroelectricity in perovskites," *Physical Review B*, vol. 65, no. 19, Article ID 195120, 2002.

[62] K. Kritayakirana, P. Berger, and R. V. Jones, "Optical spectra of ferroelectric-antiferromagnetic rare earth manganates," *Optics Communications*, vol. 1, no. 3, pp. 95–98, 1969.

[63] A. M. Kalashnikova and R. V. Pisarev, "Electronic structure of hexagonal rare-earth manganites $RMnO_3$," *JETP Letters*, vol. 78, no. 3, pp. 143–147, 2003.

[64] R. C. Rai, J. Cao, J. L. Musfeldt, S. B. Kim, S. W. Cheong, and X. Wei, "Spin-charge coupling and the high-energy magnetodielectric effect in hexagonal $HoMnO_3$," *Physical Review B*, vol. 75, no. 18, Article ID 184414, 2007.

[65] J. S. Kang, S. W. Han, J. G. Park et al., "Photoemission and x-ray absorption of the electronic structure of multifferroic $RMnO_3$ (R = Y, Er)," *Physical Review B*, vol. 71, no. 9, Article ID 092405, 2005.

[66] M. Qian, J. Dong, and D. Y. Xing, "Optical properties of the ferroelectromagnet $YMnO_3$ studied from first principles," *Physical Review B*, vol. 63, no. 15, Article ID 155101, 2001.

[67] W. S. Choi, D. G. Kim, S. S. A. Seo et al., "Electronic structures of hexagonal $RMnO_3$ (R = Gd, Tb, Dy, and Ho) thin films: optical spectroscopy and first-principles calculations," *Physical Review B*, vol. 77, no. 4, Article ID 045137, 2008.

[68] M. Fiebig, V. V. Pavlov, and R. V. Pisarev, "Second-harmonic generation as a tool for studying electronic and magnetic

structures of crystals: review," *Journal of the Optical Society of America B*, vol. 22, no. 1, pp. 96–118, 2005.

[69] C. Degenhardt, M. Fiebig, D. Fröhlich, T. Lottermoser, and R. V. Pisarev, "Nonlinear optical spectroscopy of electronic transitions in hexagonal manganites," *Applied Physics B*, vol. 73, no. 2, pp. 139–144, 2001.

[70] V. M. Axt and T. Kuhn, "Femtosecond spectroscopy in semiconductors: a key to coherences, correlations and quantum kinetics," *Reports on Progress in Physics*, vol. 67, no. 4, pp. 433–512, 2004.

[71] S. K. Sundaram and E. Mazur, "Inducing and probing non-thermal transitions in semiconductors using femtosecond laser pulses," *Nature Materials*, vol. 1, no. 4, pp. 217–224, 2002.

[72] R. D. Averitt and A. J. Taylor, "Ultrafast optical and far-infrared quasiparticle dynamics in correlated electron materials," *Journal of Physics Condensed Matter*, vol. 14, no. 50, pp. R1357–R1390, 2002.

[73] C. W. Luo, Y. T. Wang, F. W. Chen et al., "Eliminate coherence spike in reflection-type pump-probe measurements," *Optics Express*, vol. 17, no. 14, pp. 11321–11327, 2009.

[74] K. H. Wu, H. J. Chen, Y. T. Chen et al., "Marked enhancement of Néel temperature in strained $YMnO_3$ thin films probed by femtosecond spectroscopy," *Europhysics Letters*, vol. 94, no. 2, Article ID 27006, 2011.

[75] C. Thomsen, J. Strait, Z. Vardeny, H. J. Maris, J. Tauc, and J. J. Hauser, "Coherent phonon generation and detection by picosecond light pulses," *Physical Review Letters*, vol. 53, no. 10, pp. 989–992, 1984.

[76] C. Thomsen, H. T. Grahn, H. J. Maris, and J. Tauc, "Surface generation and detection of phonons by picosecond light pulses," *Physical Review B*, vol. 34, no. 6, pp. 4129–4138, 1986.

[77] H. J. Zeiger, J. Vidal, T. K. Cheng, E. P. Ippen, G. Dresselhaus, and M. S. Dresselhaus, "Theory for displacive excitation of coherent phonons," *Physical Review B*, vol. 45, no. 2, pp. 768–778, 1992.

[78] R. Merlin, "Generating coherent THz phonons with light pulses," *Solid State Communications*, vol. 102, no. 2-3, pp. 207–220, 1997.

[79] G. A. Garrett, T. F. Albrecht, J. F. Whitaker, and R. Merlin, "Coherent THz phonons driven by light pulses and the Sb problem: what is the mechanism?" *Physical Review Letters*, vol. 77, no. 17, pp. 3661–3664, 1996.

[80] A. Ghosh, J. R. Sahu, S. V. Bhat, and C. N. R. Rao, "A Raman study of multiferroic $LuMnO_3$," *Solid State Sciences*, vol. 11, no. 9, pp. 1639–1642, 2009.

[81] A. P. Litvinchuk, M. N. Iliev, V. N. Popov, and M. M. Gospodinov, "Raman and infrared-active phonons in hexagonal $HoMnO_3$ single crystals: magnetic ordering effects," *Journal of Physics Condensed Matter*, vol. 16, no. 6, pp. 809–819, 2004.

[82] J. Vermette, S. Jandl, A. A. Mukhin et al., "Raman study of the antiferromagnetic phase transitions in hexagonal $YMnO_3$ and $LuMnO_3$," *Journal of Physics Condensed Matter*, vol. 22, no. 35, Article ID 356002, 2010.

[83] J. Vermette, S. Jandl, and M. M. Gospodinov, "Raman study of spin-phonon coupling in $ErMnO_3$," *Journal of Physics*, vol. 20, no. 42, Article ID 425219, 2008.

[84] D. Lim, R. D. Averitt, J. Demsar, A. J. Taylor, N. Hur, and S. W. Cheong, "Coherent acoustic phonons in hexagonal manganite $LuMnO_3$," *Applied Physics Letters*, vol. 83, no. 23, pp. 4800–4802, 2003.

[85] P. A. Sharma, J. S. Ahn, N. Hur et al., "Thermal conductivity of geometrically frustrated, ferroelectric $YMnO_3$: extraordinary spin-phonon interactions," *Physical Review Letters*, vol. 93, no. 17, Article ID 177202, p. 1, 2004.